Magnetic and electronic structure of the film-stabilized Mott insulator BaCrO_{3}

Z. H. Zhu, F. J. Rueckert, J. I. Budnick, W. A. Hines, M. Jain, H. Zhang, and B. O. Wells

Magnetic and Electronic Structure of the Film-Stablized Mott Insulator $BaCrO_3$

Z. H. Zhu,[1] F. J. Rueckert,[1] J. I. Budnick,[1,2] W. A. Hines,[1] M. Jain,[1,2] H. Zhang,[2] and B. O. Wells[1,2]

[1]Department of Physics, University of Connecticut, Storrs, Connecticut 06269-3046, USA

[2]Institute of Material Science, University of Connecticut, Storrs, Connecticut 06269-3136, USA

(Dated: May 6, 2013)

We have synthesized and characterized laser-deposited film samples of perovskite $BaCrO_3$, a missing member of the perovskite-chromate family. The $BaCrO_3$ films have a substantially larger lattice constant than other chromates, are insulating, and exhibit weak ferromagnetism. Employing first-principles density functional theory calculations, we attribute such weak ferromagnetism to a canted C-type antiferromagnetic spin order. Additionally, comparison with the other sister compounds $CaCrO_3$ and $SrCrO_3$ suggests an anomalous Mott transition where magnetism is independent of whether the compound is metallic or insulating.

PACS numbers:

I. INTRODUCTION

Transition metal oxides (TMOs) with perovskite and related structures exhibit many fascinating electronic phenomena, including Mott insulators, metal-insulator transitions, and high-Tc superconductivity, due to transport being determined by strongly correlated d electrons.[1] One of the ubiquitous questions for these compounds is how exactly transport is coupled to magnetic degrees of freedom. The textbook situation is that ferromagnetism leads to metallic conductivity, while antiferromagnetism is associated with non-conducting behavior, particularly Mott insulators. A classic example is colossal magnetoresistance in the manganites, where a magnetic field can induce a transition from an insulating antiferromagnetic phase to a conducting ferromagnetic phase.[2] There are some exceptions which indicate other new phenomena may be in play. Observations of ferromagnetic insulators and antiferromagnetic conductors are most often explained by particular orbital orderings[3] or reduced electronic and structural dimensionality.[4] This report describes the properties of a new end member of a family that can be driven through a metal-insulator transition using chemical pressure, or bandwidth control, yet seems to retain the same magnetic structure on both sides of the transition. We have synthesized $BaCrO_3$ in perovskite form by using epitaxial film growth on an appropriate crystal template. This polymorph is apparently not stable in the bulk.

Four decades ago, a few chromate perovskites $ACrO_3$ (A = Ca, Sr, and Pb) were synthesized by several groups using solid-state reaction techniques with high pressure ($\approx$ 6-10 GPa) and high temperature ($\approx$ 1000 K).[5-9] Recent studies on $CaCrO_3$ and $SrCrO_3$ have exhibted some novel properties, drawing more attention to these chromate compounds.[10-16] For example, both of these compounds are antiferromagnetic conductors. It is also suggested that $CaCrO_3$ possibly lies in the crossover region between being itinerant and localized, implying the necessity to consider correlation effects.[14,15] An interesting orbital ordering transition and electronic phase coexistence have been discovered in $SrCrO_3$.[12]Among these chromate compounds, only $PbCrO_3$ is unambiguously thought to be an insulator with the G-type AFM spin structure. However, because of the different outer orbital configuration of Pb, $PbCrO_3$ can hardly be used to form a unified scheme to understand the exotic properties of the other chromate family compounds. On the other hand, perovskite $BaCrO_3$, which should be akin to $CaCrO_3$ and $SrCrO_3$, has not been formed as yet using traditional solid-state reaction methods. It seems that $BaCrO_3$ tends to form a hexagonal phase.[17,18] This can be understood by considering the tolerance factor $t = (r_A + r_O)/[2(r_B + r_O)]^{1/2}$, where r_A, r_B, and r_O are the ionic radii of the A, B cations, and oxygen anion, respectively.[19] Typically, perovskite structures have $t < 1$, while hexagonal polytypes result when $t > 1$. The tolerance factor of $BaCrO_3$ is 1.031, which is slightly above the allowed range for a cubic perovskite phase. Epitaxial film growth on an appropriate substrate has been known as a method for stabilizing particular phases. Here we have successfully used well lattice-matched $SrTiO_3$(STO) (001) surfaces as a template for growing perovskite $BaCrO_3$ using pulsed laser deposition (PLD) and are able to measure its basic properties.

II. EXPERIMENT

The laser target was a stoichiometric mixture of BaO and Cr_2O_3 prepared by solid-state reaction at 1000 °C in air. During growth, the substrate temperature was kept at 800 °C in 10^{-7} torr vacuum. After deposition, the films were cooled to room temperature at a rate of 4°C per minute. The film growth was found to be extremely sensitive to both the vacuum conditions and temperature of the substrate. Typically, to grow oxides one introduces oxygen into the chamber during the growth process. We found that for a large temperature range (mostly below 700 °C), with high oxygen partial pressure, the film favors the Hashemite $BaCrO_4$ structure. Under the assumption that too much oxygen might be a problem, the films then were grown under a vacuum condition and various tem-

peratures. Eventually, we were able to synthesize the perovskite $BaCrO_3$ films at 800 °C in 10^{-7} torr vacuum.

The crystal structure of the $BaCrO_3$ film was determined using both a two-circle x-ray diffractometer to study peaks perpendicular to the surface and a three-circle diffractometer with an area detector for determining in- and out-of-plane lattice constants. All of the x-ray data used Cu Kα (λ = 1.5406Å) radiation. X-ray photoemission spectroscopy (XPS) was performed in order to study the composition and purity of the $BaCrO_3$ films using a PHI Multiprobe with Al anode. Measurements of the dc magnetization were made on a Quantum Design MPMS SQUID magnetometer for temperatures 5.0 K $\leq$ T$\leq$ 300 K and magnetic fields -50 kOe $\leq$ H $\leq$ +50 kOe. Resistivity measurements were carried out using a conventional four-probe technique along with the variable temperature and magnetic field control of the MPMS. Finally, first principle calculations of the magnetic order and electronic structure of constraint representative 2x2x2 supercells of $BaCrO_3$ was carried out using the Vienna *ab* initio simulation package (VASP) [20-22]. More details of calculation can be seen in Ref. 23.
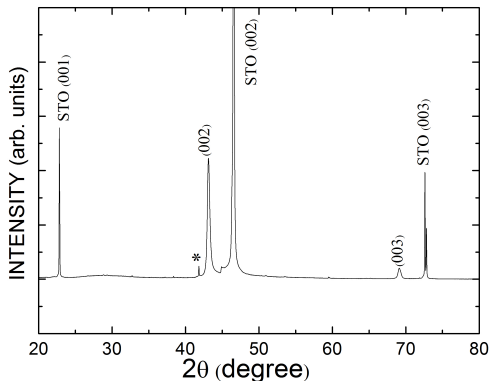

FIG. 1: X-ray diffraction pattern for a typical epitaxial $BaCrO_3$ thin film on a STO(001) substrate. The (002) and (003) $BaCrO_3$ film peaks, which occur at 43.12° and 69.09°, respectively, identify the "cubic " perovskite . The small peak labeled with (*) at 41.82° corresponds to the STO substrate (002) K$_\beta$ reflection. The small step-like feature at 44.90° is an experimental artifact related to the window size of the detector.

III. RESULTS AND DISCUSSION

Figure 1 shows the x-ray diffraction (XRD) pattern for out-of-plane peaks of a typical epitaxial $BaCrO_3$ film on a STO(001) substrate. The $BaCrO_3$ film peaks at 43.12° and 69.09° correspond to the (002) and (003) reflections, respectively, and identify the "cubic"perovskite structure. This result is unlike the case for powders where the hexagonal structure has been observed.[17,18] The lattice constants are measured on an oxford single crystal

diffractometer and give the following room-temperature values: out-of-plane lattice constant c = 4.07 Å, in-plane lattice constant a = 4.09 Å. In comparison, the pseudocubic lattice parameter for bulk $CaCrO_3$ and $SrCrO_3$ are 3.75 Åand 3.82 Å, respectively. The trend is that as the atomic number increases from Ca (20) to Ba (58), the lattice constant increases significantly. The structure of our film samples thus has a small tetragonal distortion from the cubic case. Tilting patterns in the BO_6 octahedra are common in perovskites, although in this case the associated superlattice peaks appear to be too weak to be detected from our film samples.
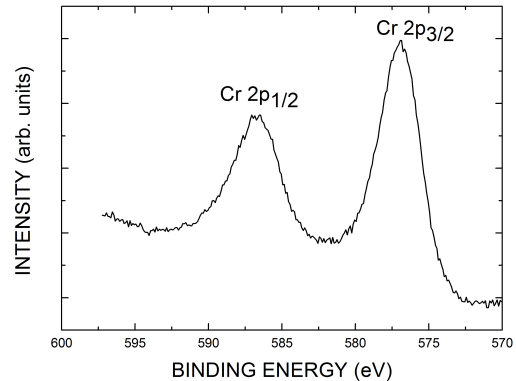

FIG. 2: X-ray photoemission spectrum for a typical epitaxial $BaCrO_3$ thin film on a STO(001) substrate. The binding energies for the Cr core level $2p_{3/2}$ and $2p_{1/2}$ peaks are 577.1 eV and 586.8 eV, respectively, consistent with the Cr^{4+} valence state for the $BaCrO_3$ film.

X-ray photoemission spectroscopy (XPS) was performed in order to study the chemical composition and phase purity of the film, along with the ionic state of Cr. No extra peaks due to impurities were observed except for that of Au, which is used for calibration and grounding of the film. The ratio between the Ba and Cr is found to be 1:1 and remains constant throughout the thickness of the film, which was revealed by collecting spectra as we sputtered through the film. A scan of the Cr 2p core level region is shown in Fig. 2. The binding energies for the $2p_{3/2}$ and $2p_{1/2}$ peaks of Cr are 577.1 eV and 586.8 eV, respectively, which matches binding energies of main peaks due to spin-orbit splitting for $CaCrO_3$, indicating the Cr^{4+} valence state in the $BaCrO_3$ films.[16] Our spectrum in Fig. 2 overall is very similar to that for $CaCrO_3$ in Ref. 16, athough we appear to have slightly poorer resolution, which does not allow us to detect the additional shoulder-like features reported in the latter

The $BaCrO_3$ films have a small, but definite magnetic response. Measurement of this signal is complicated by the small size of the film signal compared to the relatively large contribution of the substrate. Magnetic measurements were carried out for the magnetic field aligned both parallel and perpendicular to the film/substrate. For the

parallel case, the samples were mounted onto a uniform quartz rod with a very small amount of two-sided tape. For the perpendicular case, the samples were inside a small diameter plastic straw, held in place by cotton. The magnetic characteristics of a blank STO(001) substrate were measured with both orientations for temperatures 5 K ≤ T ≤ 300 K and magnetic fields -50 kOe ≤ H ≤ +50 kOe. In addition to the diamagnetic response of the STO substrate material, other background effects were present. These included: (1) trace amounts of magnetic impurities in the STO substrate material, (2) magnetic response of the cotton, which was predominately diamagnetic, and (3) trace amounts of oxygen in the SQUID sample chamber. The presence of oxygen, which can be significantly reduced but not always completely eliminated, frequently complicates low temperature magnetic measurements. Nevertheless, the various background effects were accounted for in order to isolate the magnetic response of the $BaCrO_3$ film. Fig. 3(a) shows the zero-field-cooled (ZFC) and field-cooled (FC) curves obtained for a magnetic field H = 500 Oe (H parallel) from a typical $BaCrO_3$ film on a STO(001) substrate. In order to account for the background contributions, corresponding to ZFC and FC curves at H = 500 Oe were obtained for a blank STO(001) substrate (see Fig. 3(b)). The bifurcation of the ZFC and FC curves that occurs at T ≈ 200 K for the STO substrate is attributed to magnetic impurities in the substrate material, while the small feature at T ≈ 48 K is due to trace amounts of residual oxygen in the sample chamber. Although not perfect, subtracting the subtrate curves from the corresponding total moment curves to yield the $BaCrO_3$ film curves [i.e., 3(a) - 3(b) = 3(c)] nearly removes these contributions. It can be seen in Fig. 3(c), that there is a peak in the ZFC curve for the $BaCrO_3$ thin film at T ≈25 K, below which the ZFC and FC show a significantly different temperature dependence. As discussed below, this behavior was always reproducible and is attributed to a magnetic transition associated with the $BaCrO_3$ film.

In order to explore the nature of the magnetic ordering for the $BaCrO_3$ film on a STO(001) substrate, full hysteresis loops (-50 kOe ≤ H ≤ +50 kOe) were obtained for temperatures above and below the T ≈ 25 K transition, principally for T = 300 K, 150 K, and 10 K. All of the loops obtained show a dominant diamagnetic contribution due to the STO(001) substrate along with a much smaller ferromagnetic contribution. As an example, Fig. 4(a) shows the total as-measured hysteresis loop magnetization obtained at 10 K from a sample consisting of a typical $BaCrO_3$ film on a STO(001) substrate with H parallel to the film/substrate. Fig. 4(b) shows the hysteresis loop magnetization in Fig. 4(a) with the diamagnetic part of the substrate contribution subtracted off. The resulting curve in Fig. 4(b) is characteristic of weak ferromagnetic behavior with a small coercive field and a magnetization that saturates for H ≥ 1,000 Oe. Fig. 4(c) shows the values of the saturation magnetic moment, for T = 10 K, 150 K, and 300 K, obtained

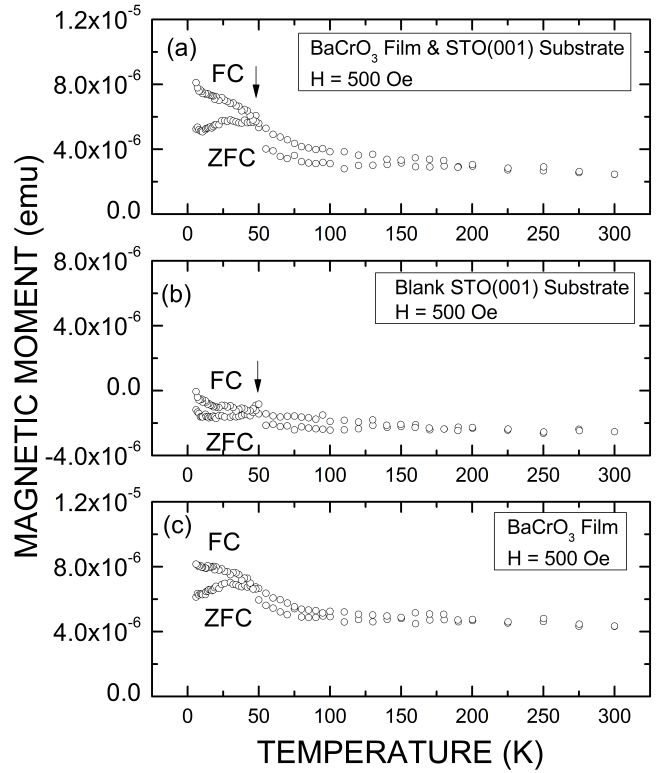

FIG. 3: Zero-field-cooled (ZFC) and field-cooled (FC) dc magnetization versus temperature for a magnetic field H = 500 Oe (H parallel) from a typical: (a) epitaxial $BaCrO_3$ thin film on a STO(001) substrate, (b) blank STO(001) substrate, and (c) epitaxial $BaCrO_3$ thin film only, obtained by subtraction. There is a peak in the ZFC curve at T ≈ 25 K, below which the ZFC and FC curves show a significant difference in temperature dependence (see Fig. 3(c)). This behavior is attributed solely to the $BaCrO_3$ film and suggests the onset of weak ferromagnetism. The bifurcation of the ZFC and FC curves that occurs at T ≈ 200 K is attributed to magnetic impurities in the substrate material, while the small feature at T ≈ 48 K is due to a trace amount of residual oxygen in the sample chamber.

from curves such as shown in Fig. 4(b). The closed (open) symbols represent values obtained for H parallel (perpendicular) to the film/substrate. The saturation magnetic moment values obtained for T = 150 K and 300 K (above the 25 K transition temperature) are the background contributions from the substrate and cotton. Similar measurements on blank substrates revealed that the background contributions were essentially temperature independent. On the other hand, the saturation magnetization values obtained at T = 10 K (below the 25 K transition temperature) shown in Fig. 4(c) include a contribution from the $BaCrO_3$ film. This behavior was reproducible in other film/substrate samples. Thus, the saturation moment for epitaxial $BaCrO_3$ film can be obtained by subtraction. Taking the saturation magnetic moment value of 0.7×10^{-5} emu (see Fig. 4(c)), with a film thickness ≈ 100 nm, the magnitude of the magnetic
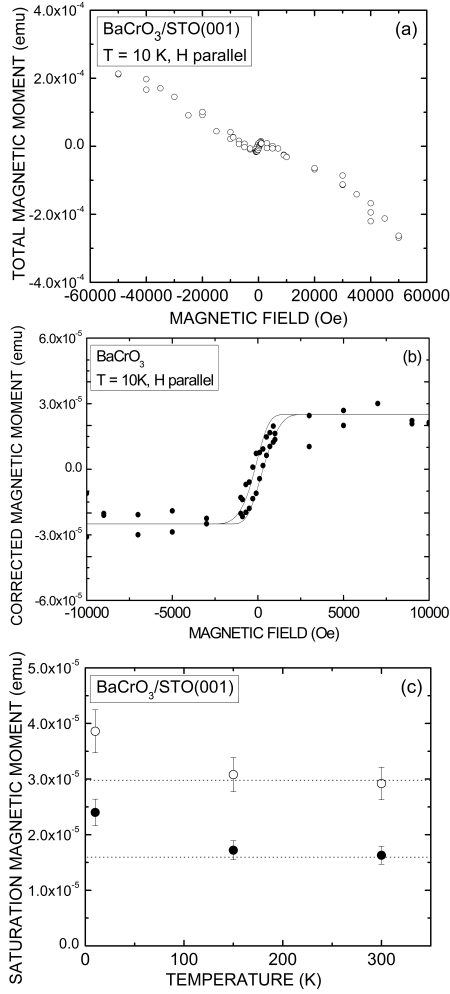
FIG. 4: (a) Hysteresis loop magnetization at 10 K for a typical $BaCrO_3$ thin film on a STO(001) substrate with H parallel to the film/substrate. The negative slope reflects the dominant diamagnetic response for the STO(001) substrate. (b) Hysteresis loop magnetization from (a) corrected for the diamagnetic contribution of the substrate. The resulting curve is characteristic of weak ferromagnetic behavior with a small coercive field and a magnetization that saturates for H $\geq$ 1,000 Oe. The solid line is a guide to the eye. (c) Saturation magnetic moment values versus temperature obtained from curves such as shown in (b). The closed (open) symbols represent values obtained for H parallel (perpendicular) to the film/substrate. The moment values obtained for T = 150 K and 300 K (above the 25 K transition temperature) are the background contributions from the substrate and cotton, while the larger moment values obtained at T = 10 K include the contribution from the $BaCrO_3$ film.

moment per Cr is estimated to be 0.028 μ_B, too small to attribute to fully ferromagnetically-aligned localized Cr^{4+} ions (2 μ_B/Cr). Instead, similar to $CaCrO_3$, it seems reasonable to attribute such weak ferromagnetism to a canted antiferromagnetic spin structure.[10,24] The rotational distortion of the CrO_6 octahedra that likely causes the measured tetragonal phase in this sample also
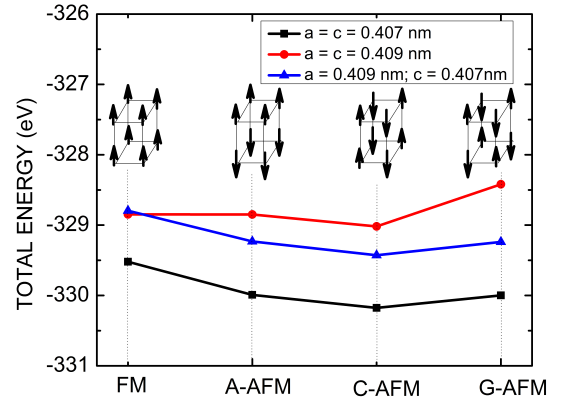

FIG. 5: (Color online) Calculated total ground state energies of four different magnetic configurations for the experimentally measured crystal structure.

allows for a Dzyaloshinsky-Moriya (DM)[25,26] interaction, similar to the case for the canted Cu^{2+} moments in La_2CuO_4. To explore the expected magnetic structure in more detail, we performed ab initio electronic structure calculations fixing the lattice to the measured structure, along with some possible variations. We explore the following magnetic configurations: ferromagnetic, A-type antiferromagnetic, C-type antiferromagnetic, and G-type antiferromagnetic. As shown in Fig. 5, for all of the structure variations explored the most favorable magnetic structure is C-type antiferromagnetism. This matches the observed and calculated magnetic structure of conducting $CaCrO_3$.[13] The calculated magnetic moment $\mu = 1.70$ μ_B/Cr for $BaCrO_3$ is greater than that of $CaCrO_3$ (1.52 μ_B/Cr calculated, 1.20 μ_B/Cr experimental), indicating a more localized behavior of Cr^{4+} in $BaCrO_3$, naturally associated with its larger lattice constant weakening the pd hybridization. Further measurements with a direct probe such as neutron diffraction would be necessary to definitely determine the magnetic structure. Our assignment of a canted C-type antiferromagnetic structure is consistent with the magnetization measurements, first principle calculations, and the related compound $CaCrO_3$.

Fig. 6(a) shows the measured $BaCrO_3$ film resistance (closed triangles) as a function of temperature revealing that $BaCrO_3$ is insulating. The variation of the resistance with temperature can be fit with the activation law $\rho = \rho_0 \exp[-\Delta/(k_B T)]$ yielding $\Delta \approx 0.38$ eV, which is smaller than that previously reported for $PbCrO_3$ ($\approx$ 0.5 eV).[14] However, our electronic calculation for C-type AFM $BaCrO_3$ using a spin polarized local density approximation (LSDA) as shown in Fig. 6(b) exhibits a metallic behavior. Conductivity is more difficult to describe by ab initio methods than ground state magnetic structure but when the primary difficulty is the strength of electronic correlations in compounds with partially filled d bands an LSDA+U calculation may capture the basic electronic state. For these calculations, we chose J = 0.87 eV and U = 3 eV as calculated for
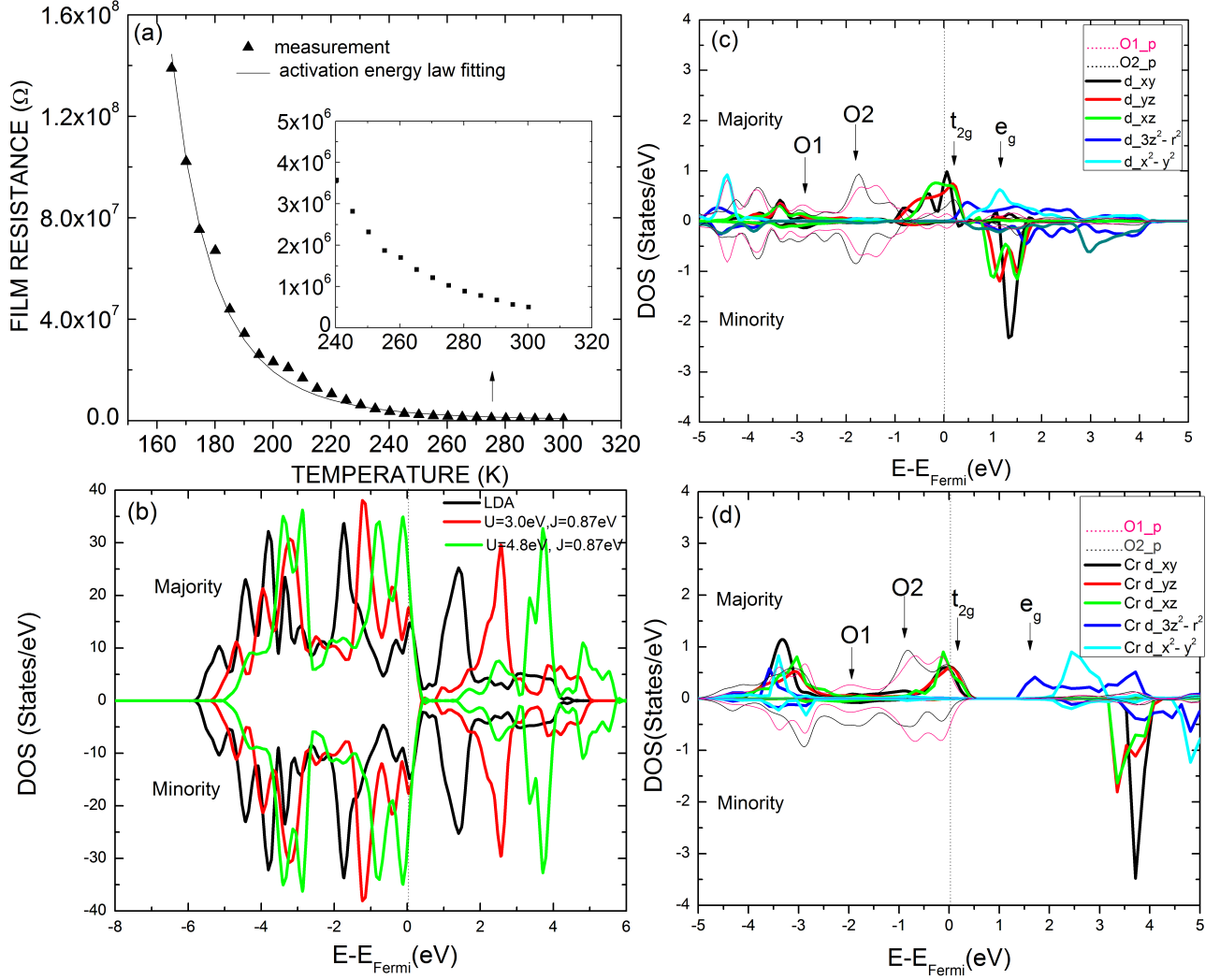
FIG. 6: (Color online) (a) Resistance versus temperature for a typical epitaxial $BaCrO_3$ thin film on a STO(001) substrate: closed triangles -measured values and solid line - fit to activation law yielding an energy parameter $\Delta \approx 0.38$ eV. (b) Total density of states (TDOS) of $BaCrO_3$ with room temperature crystal structure and C-type AFM spin order using LSDA and LSDA+U. (c) and (d) Projected density of states (PDOS) of the d orbital of Cr atom and the p orbital of O atom calculated by LSDA and LSDA+ U (U = 4.8 eV, J = 0.87 eV) in C-AFM order, where O1 and O2 represent in-plane and apical O atoms, respectively.

CrO_2 and $CaCrO_3$, respectively.[13,27] We included another calculation with a larger U = 4.8 eV based on a recent experimental report on $CaCrO_3$ using resonant photoemission.[16] As shown in Fig. 6(b) the ground state remains metallic within Coulomb corrections, which conflicts with our experimental observations. To further elucidate the emergence of a gap opening above the Fermi level after introducing a Coulomb correction, projected density of states (PDOS) of the d orbital of Cr atom and the p orbital of O atom are calculated by using LSDA and LSDA+U, shown in Fig. 6(c) and Fig. 6(d), respectively. It can be seen that the gap opening stems from the splitting between the t_{2g} and the e_g orbitals of the Cr due to the Coulomb interaction. However, the

Fermi energy still lies in the t_{2g} orbitals of Cr and p orbitals of O, yielding a metallic state, which is similar to the theoretical study of $SrCrO_3$.[28] The slight difference in the p orbitals of apical O and in-plane O reflects the tetragonal phase of crystal. The fact that the LSDA+U calculation still does not reveal the insulating nature of the real compound may simply be due to the electron correlations being too strong to properly capture the essential physics in a Hartree-Fock approximation. There may also be further effects not included in this calculation. For example, the Jahn-Teller (JT) effect has proven to be essential to understanding conductivity in some oxides. In $LaMnO_3$, even when using a more sophisticated LDA+DMFT approach, the insulating be-

havior appears only when JT distortion and Coulomb correction work together.[29] The ionic radii range from Ca^{2+} to Ba^{2+}: $r(Ca^{2+}(VIII)) = 1.12$ Å, $r(Sr^{2+}(VIII)) = 1.26$ Å, $r(Pb^{2+}(VIII)) = 1.29$ Å, $r(Ba^{2+}(VIII)) = 1.42$ Å.[30] Correspondingly, the pseudocubic lattice parameter of the compound also increases, $a_c(Ca) = 3.75$ Å, $a_c(Sr) = 3.82$ Å, $a_c(Pb) = 4.00$ Å, and $a_c(Ba) = 4.07$Å. Due to the fully-filled orbital configurations of Ca^{2+}, Sr^{2+}, and Ba^{2+}, the electronic structures of these chromate compounds are mainly determined by the corner-sharing CrO_6 octahedra. Therefore, one might think that the electronic phases of these chromate compounds, ranging from metallic to insulating, could be understood in a unified scheme, namely, a variation of the ionic radius modifies the octahedral unit cell, resulting in a Mott transition. However, the Mott transition is expected to be accompanied by a nonmagnetic to antiferromagnetic transition while similar materials, such as manganites, undergo a ferromagnetic to antiferromagnetic transition. In this case, the magnetism appears mostly unaffected by the conductivity change of the samples; an unexpected result. Thus the set of compounds $CaCrO_3$, $SrCrO_3$, and $BaCrO_3$ are a good model family for exploring more subtle aspects of a bandwidth controlled Mott transition especially the detailed connection between the magnetic structure and conductivity.

IV. SUMMARY

In conclusion, we report the epitaxial growth of a $BaCrO_3$ film with the perovskite structure, which to date has not been obtained in the powder samples made by standard solid-state synthesis techniques. This material, exhibiting weak ferromagnetism which is possibly due to a canted antiferromagnetic spin structure, has much in common with other chromate family members and should serve as an important example for understanding the magnetic and electronic structure of the TMOs.

ACKNOWLEDGMENTS

[1] M. Imada, A. Fujimori, and Y. Tokura, Rev. Mod. Phys. 70, 1039-1263 (1998).

[2] P. Schiffer, A. P. Ramirez, W. Bao, and S. -W. Cheong, Phys. Rev. Lett. 75, 3336 (1995).

[3] D. I. Khomskii and G. A. Sawatzky, Solid State Commun. 102, 87 (1997).

[4] Y. Yoshida, S. I. Ikeda, H. Matsuhata, N. Shirakawa, C. H. Lee and S. Katano, Phys. Rev. B 72, 054412 (2005).

[5] B. L. Chamberland and C. W. Moeller, J. Solid State Chem. 5, 39 (1972).

[6] B. L. Chamberland and C. W. Moeller, Solid State Commun. 5, 663 (1967).

[7] J. B. Goodenough, J. M. Long, and J. A. Kafalas, Mater. Res. Bull. 3, 471 (1968).

[8] J. F. Weiher, B. L. Chamberland, and J. L. Gillson, J. Solid State Chem. 5, 39 (1972).

[9] W. L. Roth and R. C. DeVires, J. Appl. Phys. 38, 951 (1967).

[10] J. S. Zhou, C. -Q. Jin, Y. -W. Long, L. -X. Yang, and J. B. Goodenough, Phys. Rev. Lett. 96, 046408 (2006).

[11] A. J. Williams, A. Gillies, and J. P. Attfield, G. Heymann, H. Hupertz, M. J. Martinze-Lope, and J. A. Alonso, Phys. Rev. B 73, 104409 (2006).

[12] L. Ortega-San-Martin, A. J. Williams, J. Rodgers, J. P. Attfield, G. Heymann, and H. Huppertz, Phys. Rev. Lett. 99, 255701 (2007).

[13] A. C. Komarek, S. V. Streltsov, M. Isobe, T. Moller, M. Hoelzel, A. Senyshyn, D. Trots, M. T. Fernandez-Diaz, T. Hansen, H. Gotou, T. Yagi, Y. Ueda, V. I. Anisimov, M. Gruninger, D. I. Khomskii, and M. Braden, Phys. Rev. Lett. 101, 167204 (2008).

[14] S. V. Streltsov, M. A. Korotin, V. I. Anisimov, and D. I. Khomskii, Phys. Rev. B 78, 054425 (2008).

[15] A. C. Komarek, T. Moller, M. Isobe, Y. Drees, H. Ulbrich, M. Azuma, M. T. Fernandez-Diaz, A. Senyshn, M. Hoelzel, G. Andre, Y. Ueda, M. Gruninger, and M. Braden, Phys. Rev. B 84, 125114 (2011).

[16] P. A. Bhobe, A. Chainani, M. Taguchi, R. Eguchi, M. Matsunami, T. Ohtsuki, K. Ishizaka, M. Okawa, M. Oura, Y. Senba, H. Ohashi, M. Isobe, Y. Ueda, and S.Shin, Phys. Rev. B 83, 165132 (2011).

[17] B. L. Chamberland, J. Solid State Chem. 43, 3 (1982).

[18] P. S. Haradem, B. L. Chamberland, L. Katz, J. Solid State Chem. 1, 34 (1979).

[19] C. -Q. Jin, J. S. Zhou, J. B. Goodenough, Q. Q. Liu, J. G. Zhao, L. X. Yang, Y. Yu, R. C. Yu, T. Katsura, A. Shatskiy, and E. Ito, Proc. Natl. Acad. Sci. USA, 105, 7115 (2008).

[20] G. Kresse and J. Furthmuller, Phys. Rev. B 54, 11169 (1996).

[21] G. Kresse and J. Furthmuller, Comput. Mater. Sci. 6, 15 (1996).

[22] G. Kresse and J. Hafner, J. Phys.: Condens. Matter 6, 8245 (1994).

[23] Z. H. Zhu and X. H. Yan, J. Appl. Phys. 106, 023713 (2009).

[24] O. Ofer, J. Sugiyama, M. Mansson, K. H. Chow, E. J. Ansaldo, J. H. Brewer, M. Isobe, and Y. Ueda, Phys. Rev. B 184405 (2010).

[25] I. Dzyaloshinsky, J. Phys. Chem. Solids 4, 241 (1958).

[26] T. Moriya, Phys. Rev. 120, 91 (1960).

[27] M. A. Korotin, V. I. Anisimov, D. I. Khomskii and G. A. Sawatzky, Phys. Rev. Lett. 80, 4305 (1998).

[28] K. -W. Lee and W. E. Pickett, Phys. Rev. B 80, 125133 (2009).

[29] A. Yamasaki, M. Feldbacher, Y.-F. Yang, O. K. Andersen, and K. Held, Phys. Rev. Lett. 96, 166401 (2006).

[30] R. D. Shannon, Acta Crystalloger. Sect. A 32, 751 (1976).